

# Molecular Dynamics Simulations of the Ionic Liquid 1-*n*-Butyl-3-Methylimidazolium Chloride and Its Binary Mixtures with Ethanol

Mo Chen,<sup>||,⊥,†</sup> Robert Pendrill,<sup>‡,⊥</sup> Göran Widmalm,<sup>‡</sup> John W. Brady,<sup>†</sup> and Jakob Wohlert\*,<sup>§</sup>

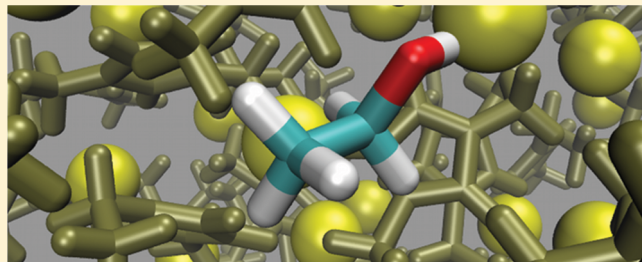
<sup>†</sup>Department of Food Science, Cornell University, Ithaca, New York 14853, United States

<sup>‡</sup>Department of Organic Chemistry, Arrhenius Laboratory, Stockholm University, SE-10691 Stockholm, Sweden

<sup>§</sup>Wallenberg Wood Science Center, KTH Royal Institute of Technology, SE-10044 Stockholm, Sweden

## Supporting Information

**ABSTRACT:** Room temperature ionic liquids (ILs) of the imidazolium family have attracted much attention during the past decade for their capability to dissolve biomass. Besides experimental work, numerous computational studies have been concerned with the physical properties of both neat ILs and their interactions with different solutes, in particular, carbohydrates. Many classical force fields designed specifically for ILs have been found to yield viscosities that are too high for the liquid state, which has been attributed to the fact that the effective charge densities are too high due to the lack of electronic polarizability. One solution to this problem has been uniform scaling of the partial charges by a scale factor in the range 0.6–0.9, depending on model. This procedure has been shown to improve the viscosity of the models, and also to positively affect other properties, such as diffusion constants and ionic conductivity. However, less attention has been paid to how this affects the overall thermodynamics of the system, and the problems it might create when the IL models are combined with other force fields (e.g., for solutes). In the present work, we employ three widely used IL force fields to simulate 1-*n*-butyl-3-methylimidazolium chloride in both the crystal and the liquid state, as well as its binary mixture with ethanol. Two approaches are used: one in which the ionic charge is retained at its full integer value and one in which the partial charges are uniformly reduced to 85%. We investigate and calculate crystal and liquid structures, molar heat capacities, heats of fusion, self-diffusion constants, ionic conductivity, and viscosity for the neat IL, and ethanol activity as a function of ethanol concentration for the binary mixture. We show that properties of the crystal are less affected by charge scaling compared to the liquid. In the liquid state, transport properties of the neat IL are generally improved by scaling, whereas values for the heat of fusion are unaffected, and results for the heat capacity are ambiguous. Neither full nor reduced charges could reproduce experimental ethanol activities for the whole range of compositions.



## 1. INTRODUCTION

Ionic liquids (ILs) are salts, composed of organic cations and organic or inorganic anions, which melt at relatively low temperatures. They have almost negligible vapor pressures and as a consequence very low flammability. In addition, they are recyclable and can, by varying the composition, be designed for specific purposes, such as reaction medium for chemical synthesis or catalysis and, indeed, solvation.<sup>1</sup>

In 2002, the group of R. Rogers discovered that 1-*n*-butyl-3-methylimidazolium chloride ([BMIM]Cl, see Figure 1) was capable of dissolving lignocellulosic biomass at a solubility of up to 25% (wt %), a much higher extent than in both aqueous solvents and most of the traditional organic solvents.<sup>2</sup> Since

then, a large number of ILs capable of dissolving cellulose and related carbohydrates have been found.<sup>3</sup> Today, biomass is still one of the most under-utilized natural resources, but this may change as new technologies based on processing with ionic liquids followed by selective precipitation of its constituents: cellulose, hemicellulose, and lignin, become accessible.<sup>4,5</sup>

The use of molecular dynamics (MD) simulations to study ionic liquids has a long history, dating back to at least the 1970s.<sup>6</sup> These early studies were primarily of a more general theoretical kind, but in 2002, just about the same time as when Rogers and co-workers dissolved cellulose in [BMIM]Cl,<sup>2</sup> the first general force field for ionic liquids containing imidazolium cations was published, with a strong commitment to the development of new “green” technologies.<sup>7</sup> In 2004 Canongia Lopés et al. published the first in a series of papers describing a general force field for imidazolium-based ILs based on a combination of the OPLS-AA<sup>8</sup> and AMBER<sup>9</sup> potentials,<sup>10</sup> and

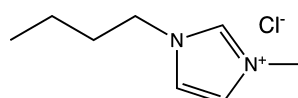


Figure 1. Chemical structure of [BMIM]Cl.

Received: March 31, 2014

in the same year, Liu et al. published a force field for imidazolium ions based solely on the AMBER potential.<sup>11</sup> These two force fields have since become two of the most used parameter sets for IL simulations: but they are of course not the only ones. During the past decade, several atomic force fields for MD simulations of ILs have been developed (see, e.g., Dommert et al.<sup>12</sup> for a recent review). All force fields have been validated, to some extent, by comparing calculated densities, heats of vaporization, translational self-diffusion coefficients, shear viscosities, etc. from MD simulations with the, sometimes scarce, experimental data available. Unfortunately, specifically for the case of ILs comprised of imidazolium-based cations in combination with halide anions, none of these force fields completely reproduced all experimental results. In particular, it was found that transport properties (self-diffusion and ion conductivity) usually were severely underestimated,<sup>13,14</sup> especially for smaller anions. It was suggested that the reason for this is that the electrostatic interactions become overestimated in classical atomic models, leading to a pronounced charge ordering effect, and that this is a consequence of neglecting both the dynamic electronic polarizability and charge transfer between the ions.<sup>14</sup>

Indeed, it has been shown that force fields that take into account the dynamic electronic polarization effects can represent these molten salts more realistically. As an example, a polarizable force field for 1-ethyl-3-methylimidazolium nitrate presented excellent agreement with experiments in terms of shear viscosity and diffusion.<sup>15</sup> More recently, Borodin<sup>16</sup> developed a general many-body polarizable force field, which reproduced thermodynamic and transport properties of a series of ILs very well. However, these polarizable force fields come at a significantly higher computational cost than conventional nonpolarizable force fields and are not presently practical solutions for large-scale MD simulations.

An alternative approach was proposed by Köddermann and co-workers.<sup>17–19</sup> They show that it is possible to reproduce experimental self-diffusion coefficients, heats of vaporization, and NMR relaxation times for the ILs  $[C_n\text{MIM}]^+[\text{NTf}_2]^-$  by optimization of the van der Waals interactions. The resulting force field was also shown to work well for mixtures with organic solvents.<sup>20</sup> Also, the specific functional form of the repulsion-dispersion potential has been shown to influence calculated transport properties, which was successfully utilized<sup>21–23</sup> in the parametrization of nonpolarizable force fields for several ILs employing integer charges.

Ab initio calculations on isolated ion pairs, as opposed to using single ions, reveal a significant effect from charge transfer. Bühl and co-workers<sup>24</sup> found that using this approach on 1,3-dimethylimidazolium chloride ( $[\text{MMIM}]^+\text{Cl}^-$ ) the total charge on the ions dropped to around  $\pm 0.7e$ . Inspired by this, Youngs and Hardacre<sup>14</sup> applied uniform scaling of charges in their model for  $[\text{MMIM}]^+\text{Cl}^-$  in a systematic way, and found that a total charge around  $\pm 0.7e$  significantly improved the results for the self-diffusion, while the structural properties were less affected. Since then, the use of noninteger ionic charges has been found to improve models for a wide range of ionic liquids,<sup>12</sup> either by uniform scaling, treating the ion charge as yet another variable force field parameter,<sup>14,25,26</sup> or by a reduction based on specific ab initio calculations.<sup>27–31</sup> In addition, Leontyev et al. have proposed to use a charge-scaling factor of about 0.7 in MD simulations of ions in general.<sup>32</sup>

A reduction of partial charges in simulations of ionic liquids has emerged as an attractive alternative to more expensive

computational approaches, and, as mentioned above, it does have a theoretical foundation as far as neat ionic liquid systems are considered. However, using these scaled potentials in combination with solutes (e.g., carbohydrates) might be problematic, for instance in the sense that it is not totally obvious whether or not the scaling should apply to the solute as well, or if the scale factor should vary with solute concentration. Nevertheless, Moyna and co-workers studied cellobiose dissolution in  $[\text{BMIM}]^+\text{Cl}^-$  using a uniform charge reduction of 0.73 for the ions,<sup>33,34</sup> and Youngs et al. studied glucose in  $[\text{EMIM}]^+\text{OAc}^-$  using a scale-factor of 0.85.<sup>35</sup> Also, Liu's force field<sup>11</sup> has been used to study IL/carbohydrate interactions. Zhao et al. used it to study cellulose dissolution in various ILs,<sup>36–38</sup> and Xu et al. investigated cellulose in  $[\text{BMIM}]^+\text{Cl}^-$  using the same force field, but with the partial charges scaled according to the work by Chaban et al.<sup>26</sup> In addition, Gross and co-workers have developed a CHARMM-compatible force field to study cellulose dissolution in  $[\text{BMIM}]^+\text{Cl}^-$ ,<sup>39,40</sup> which so far only has been used with integer ionic charges.

In the present study, three atomic, nonpolarizable, force fields that have recently been used to explicitly study IL/carbohydrate interactions and cellulose dissolution in ILs are examined. The main purpose was to investigate how well they reproduce experimental data for the neat IL as well as thermodynamic data for the solvation of polar solutes, and how this is affected by a uniform scaling of partial charges. To that end, we have performed extensive MD simulations to study the IL  $[\text{BMIM}]^+\text{Cl}^-$  in both the solid and the liquid phase, as well as its binary mixtures with ethanol, at varying compositions. The solid phase is characterized using crystal lattice parameters and molar heat capacity (with quantum-mechanical correction terms). The liquid phase is characterized by its thermodynamic (density, QM-corrected molar heat capacity), structural (radial and spatial distribution function) and dynamical properties (shear viscosity, self-diffusion, and ionic conductivity). Finally, the binary mixture of  $[\text{BMIM}]^+\text{Cl}^-$  and ethanol is investigated by its density and ethanol activity, as a function of composition. All properties are compared to experimental data, where available.

## 2. THEORY AND METHODS

### 2.1. Quantum Mechanical Correction to the Heat Capacity.

The (molar) heat capacity at constant pressure,  $C_p$ , can be related to the heat capacity at constant volume,  $C_v$  via the exact thermodynamic relation

$$C_p - C_v = \Delta C = VT \frac{\alpha_p^2}{K_T} \quad (1)$$

where  $V$  is the molecular volume,  $\alpha_p$  is the volumetric thermal expansion coefficient, and  $K_T$  is the isothermal compressibility.  $\alpha_p$  and  $K_T$  can be determined experimentally, or they can be computed from fluctuations in enthalpy  $H$  and volume (see, e.g., Caleman et al.<sup>41</sup>):

$$\langle \delta V \delta H \rangle = k_B T^2 \langle V \rangle \alpha_p \quad (2)$$

$$\langle \delta V^2 \rangle = k_B T \langle V \rangle K_T \quad (3)$$

In classical thermodynamics,  $C_v$  and  $C_p$  are related to fluctuations in energy and enthalpy through

$$C_v^{\text{class}} = \langle \delta U^2 \rangle / k_B T^2 \quad (4)$$

$$C_p^{\text{class}} = \langle \delta H^2 \rangle / k_B T^2 \quad (5)$$

which can be calculated from constant volume or constant pressure MD simulations. However, this method will greatly overestimate  $C_p$ , at room temperature and below, due to the fact that a large part of  $C_p$  comes from vibrations that to some extent are quantum mechanical.

One way of correcting for quantum mechanical effects was proposed by Berens et al.<sup>42</sup> They considered the distribution of normal modes, or density of states (DoS), as a function of normal-mode frequency  $\nu$ , which can be calculated from the Fourier transform of the mass-weighted atomic velocity autocorrelation functions (see refs 41–44 for details). The distribution should be normalized such that

$$\int_0^\infty \text{DoS}(\nu) d\nu = 3N \quad (6)$$

where  $N$  is the total number of degrees of freedom present in the system. If one approximates each normal mode as a quantum mechanical harmonic oscillator with frequency  $\nu_i$ , the contribution to the heat capacity from each such oscillator is

$$k_B \left( \frac{h\nu_i}{k_B T} \right)^2 \frac{\exp(h\nu_i/k_B T)}{[\exp(h\nu_i/k_B T) - 1]^2} = k_B W(\nu_i) \quad (7)$$

In the classical limit (large  $T$ ), Dulong–Petit's law is regained ( $k_B$  per degree of freedom), while the expression goes to zero when  $T$  is small. Thus, a quantum mechanical correction to the classical heat capacity may be approximated as<sup>42</sup>

$$\delta C_V^{\text{qm}} = k_B \int_0^\infty (W(\nu) - 1) \text{DoS}(\nu) d\nu \quad (8)$$

The final expression for the quantum-corrected heat capacity becomes

$$C_p^{\text{corr}} = C_V^{\text{class}} + \delta C_V^{\text{qm}} + \Delta C = C_p^{\text{class}} + \delta C_V^{\text{qm}} \quad (9)$$

Such corrections have been successfully applied before to, for example, liquid water,<sup>42</sup> ice,<sup>45</sup> and carbohydrates.<sup>46</sup>

**2.2. Computational Details.** **2.2.1. Force Fields.** In the present study, three atomic force fields for [BMIM]Cl were used. They include a CHARMM-based forced field parametrized by Gross, Bell, and Chu<sup>39</sup> (referred to as GBC), an Amber-based force field derived by Liu, Huang, and Wang<sup>11</sup> (referred to as LHW), and an OPLS-AA force field developed and improved by Canongia Lopes, Dechamps, and Pádua (referred to as CLDP).<sup>10,47</sup> To investigate the effects of uniform scaling of partial charges, the above force fields were used in two versions, one with the partial charges retained at their original values and one where they were scaled to 85%. This is a smaller scaling than has been used for CLDP before, but since the other two force fields have not been investigated in this respect before, and moreover as the purpose of the present study is not to optimize potential parameters but rather to study the effect of charge-scaling in general, this value was chosen as a compromise.

The potential parameters for ethanol were taken from the CHARMM General Force Field (CGenFF)<sup>48</sup> (combined with the GBC model for [BMIM]Cl), the General Amber Force Field (GAFF)<sup>49</sup> with partial charges from Fox and Kollman<sup>50</sup> (with the LHW model), and the OPLS-AA force field<sup>8</sup> (with the CLDP model). The ethanol models were always used with their respective partial charges intact; that is, no scaling was applied.

**2.2.2. Molecular Dynamics Simulations.** In the present work, two different MD simulation programs were used.

GROMACS 4.6<sup>51</sup> was used for simulations for  $C_p$  calculations in both the liquid and the solid phase, as well as IL/ethanol binary mixtures. To study transport properties in the liquid state, as well as crystal and liquid structures, simulations were performed using CHARMM v35b4.<sup>52</sup> Care was taken to ensure that the implementations of the force fields produced the same results with both programs and that the simulation protocols were as close to identical as possible.

All simulations were performed in an NPT ensemble using a basic time step of 2 fs, unless otherwise noted. Electrostatics was handled with the PME method<sup>53,54</sup> using a real-space cutoff of 1 nm. Lennard-Jones interactions were gradually switched to zero<sup>55</sup> between 0.8 and 1.2 nm in the case of GROMACS, and between 1.0 and 1.2 nm with CHARMM. Temperature was maintained at the desired target temperature using a Nosé–Hoover thermostat,<sup>56,57</sup> and pressure was kept at 1 atm using a Parrinello–Rahman barostat<sup>58</sup> in the case of GROMACS, and the extended system method<sup>57,59</sup> in the case of CHARMM. All bonds were kept at their equilibrium values using LINCS<sup>60</sup> and SHAKE<sup>61</sup> with GROMACS and CHARMM, respectively, except for the simulations that were used for normal-mode analysis, in which case a fully flexible model was employed. Normal mode distributions for both the crystal and liquid phases were calculated from the atomic velocity autocorrelation functions using the GROMACS utility program g\_dos.<sup>41</sup> The simulations used for the DoS calculations extended to 100 ps and were run at constant volume and temperature, with fully flexible bonds, and with all atomic velocities saved every 4 fs, using a basic time step of 0.5 fs. Liquid structure, diffusion, and conductivity was based on 100 ns simulations (after 5 ns of equilibration) with all atomic positions saved every 2 ps, and viscosity was calculated from 5 ns simulations starting from 10 evenly spaced restart-points taken from the last half of the 100 ns trajectory, with the full pressure tensor saved every step.

For simulations of the liquid, a system of 200 ion pairs was used, and for the crystal,  $3 \times 3 \times 3 = 27$  unit cells ( $Z = 4$ ) were used, resulting in 108 ion pairs.

The simulations carried out to calculate activity coefficients consisted of [BMIM]Cl/ethanol mixtures corresponding to ethanol mole fractions of 0.005 (1 ethanol molecule and 200 ion pairs), 0.25 (30/90), 0.40 (50/75), 0.50 (75/75), 0.60 (75/50), 0.75 (150/50), and 1.00 (300 ethanol molecules). The chemical potential of ethanol in each mixture was calculated by thermodynamic integration, in which all intermolecular interactions between one ethanol molecule and the rest of the system was linearly switched off by means of a coupling parameter  $\lambda$ , where  $\lambda = 1$  means all interactions intact, and  $\lambda = 0$  means the fully decoupled state. To avoid singularities at  $\lambda = 0$ , soft-core potentials<sup>62</sup> were employed. Furthermore, the intramolecular interactions were always kept intact, meaning that the decoupled state corresponded to the vapor phase. Simulations were performed at constant  $\lambda$  at 25 different values between 0 and 1. Each simulation was 5 ns in length, of which the last 4.5 ns were used for analysis. The value of  $dG/d\lambda$  was recorded every 10 steps, and the final integration was performed using BAR.<sup>63</sup> To speed up the convergence of the simulations, replica exchange molecular dynamics (REMD)<sup>64</sup> was employed. Four replicas at temperatures 350, 375, 400, and 425 K were run simultaneously, and exchanges between neighboring replicas were attempted every 10 steps. The acceptance ratio in this setting was around 1/100, leading to around 1000 successful exchanges for each replica in each direction during the course of a simulation. REMD was also

used to calculate densities at 298 K of the two mixtures with lowest ethanol mole fraction ( $x = 0.15$  and  $x = 0.25$ ). In this case, four replicas with temperatures 298, 325, 350, and 375 K were used, with approximately the same acceptance ratio as above. For the higher mole fractions ( $x \geq 0.4$ ) only one simulation each at the desired temperature was performed.

### 3. RESULTS AND DISCUSSION

**3.1. Solid State.** The crystal structure of [BMIM]Cl has been characterized using X-ray diffraction and differential scanning calorimetry.<sup>65,66</sup> It was found to exist in two different polymorphs; one with an orthorhombic and one with a monoclinic crystal unit cell<sup>65</sup> (see Figure 2). Based on its higher

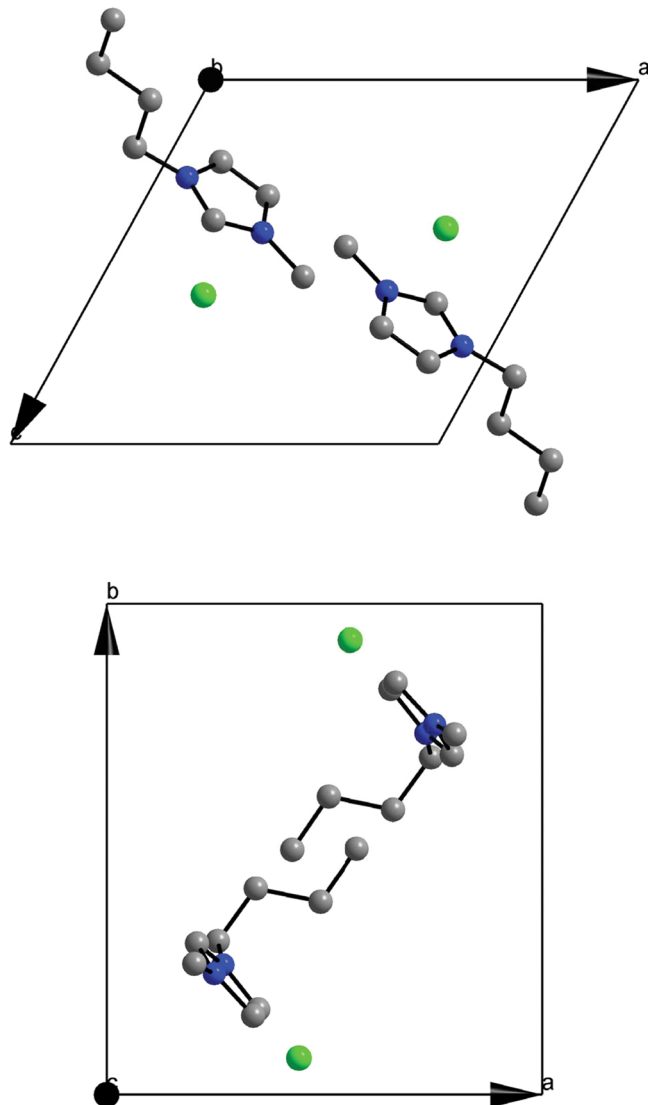


Figure 2. Crystal structures of BMIM[Cl]. Monoclinic (top) and orthorhombic (bottom).

melting point, 66 °C compared to 41 °C, the orthorhombic structure was determined to be more thermodynamically stable. Furthermore, it was found that [BMIM]Cl would only crystallize into its monoclinic form in the presence of a second solvent or solute species.<sup>65</sup>

The structure of the monoclinic polymorph<sup>66</sup> was downloaded from the Cambridge Structural Database (CSD, ID

213959), and the orthorhombic structure<sup>65</sup> was taken from the original reference, and simulated under *NPT* conditions. The temperatures used for studying the structure were 173 and 293 K for the orthorhombic and monoclinic structures respectively, which are the same as in the actual X-ray experiments. Molar heat capacities were calculated at 298 K. All simulations were performed at atmospheric pressure.

Simulations showed that both structures were stable with all force fields. To quantify the agreement between simulated and experimental structures, a lattice root-mean-square deviation, RMSD, was calculated in the following way. For each of the three lattice parameters  $a$ ,  $b$ , and  $c$ , the three angles  $\alpha$ ,  $\beta$ , and  $\gamma$ , the relative deviation from the experimental value was calculated from 10 ns of simulation data (see Supporting Information Tables S1 and S2). The RMSD was then calculated with respect to these six values. The results for each force field, charge distribution, and crystal polymorph are displayed in Figure 3.

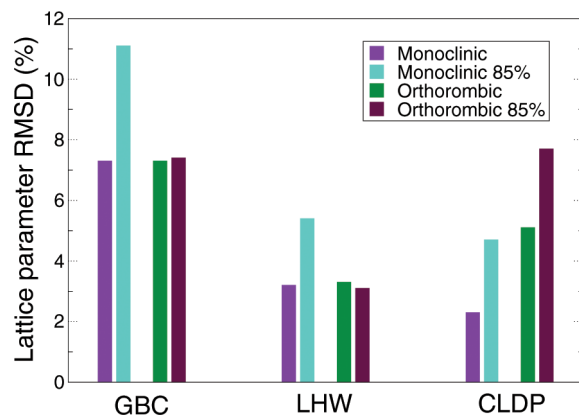


Figure 3. Lattice RMSD in percent for the three different force fields and the two different crystal structures at  $T = 173$  K for the orthorhombic structure, and  $T = 293$  K for the monoclinic structure.

Figure 3 shows that the force field that gives the overall smallest RMSD is LHW, whereas GBC gives the largest. Furthermore, for GBC and LHW the monoclinic structure is more sensitive to the partial charges than the orthorhombic. A reduction to 85% increases the RMSD for the monoclinic structure by around 1%, whereas the orthorhombic is unaffected. For CLDP, however, both structures are affected by approximately the same amount.

The molar heat capacity at constant pressure,  $C_p$ , of [BMIM]Cl has been determined experimentally<sup>67–69</sup> at  $T = 298$  K to  $275.98\text{--}322.7 \text{ J mol}^{-1} \text{ K}^{-1}$ . Here,  $C_p$  at  $T = 298$  K for each of the two polymorphs was calculated using eq 9 for each of the three force fields, both with full and scaled charges. The classical value,  $C_p^{\text{class}}$ , was calculated from enthalpy fluctuations in a 10 ns long trajectory, employing bond constraints. Since the bond potentials are harmonic, they contribute  $k_B$  to the heat capacity each. In principle, there exist couplings between bond vibrations and other modes that contribute to the heat capacity. In the present case, by comparing trial simulations with and without bond constraints, these were found to be negligible. Thus, a term  $N_c k_B$  to  $C_p^{\text{class}}$  was added to the result, where  $N_c$  is the number of constraints. The classical heat capacity from the simulations was much higher than the experimental ones. Thus, a quantum mechanical correction to the classical heat capacity

**Table 1.** Molar Heat Capacity of Solid [BMIM]Cl in  $\text{J mol}^{-1} \text{K}^{-1}$ <sup>a</sup>

	full charges			scaled charges		
	GBC	LHW	CLDP	GBC	LHW	CLDP
Orthorhombic						
$\delta C_V^{\text{qm}}$	-434.2	-441.2	-427.3	-432.5	-439.2	-425.9
$\Delta C$	29.5	20.5	27.9	31.8	22.3	28.6
$C_V^{\text{class}}$	647.6	635.0	649.0	644.4	635.9	647.8
$C_P^{\text{class}}$	677.1	655.5	676.9	676.2	658.2	676.4
$C_P^{\text{corr}}$	242.9 (10.1)	214.3 (9.0)	249.6 (9.5)	243.7 (6.3)	219.1 (9.8)	250.6 (7.9)
Monoclinic						
$\delta C_V^{\text{qm}}$	-433.2	-439.2	-425.1	-430.7	-438.3	-425.5
$\Delta C$	22.6	17.7	21.2	24.4	21.2	26.9
$C_V^{\text{class}}$	656.1	641.0	652.5	656.7	642.1	648.4
$C_P^{\text{class}}$	678.7	658.7	673.7	681.1	663.3	675.3
$C_P^{\text{corr}}$	245.5 (7.5)	219.4 (7.5)	248.6 (8.3)	250.4 (10.3)	224.9 (16.9)	249.8 (8.2)

<sup>a</sup>The quantum mechanical correction term,  $\delta C_V^{\text{qm}}$  is calculated by integrating over the normal mode distribution (eq 8), and  $\Delta C$  is calculated using eq 1, with  $\alpha_p$  and  $K_T$  calculated from simulations using eq 2 and eq 3. The classical heat capacity at constant volume is calculated as  $C_V^{\text{class}} = C_P^{\text{class}} - \Delta C$ , which gives excellent agreement with  $C_V$  calculated from additional simulations performed at constant  $NVT$  (data not shown). Finally, the corrected molar heat capacity is calculated as  $C_P^{\text{corr}} = C_P^{\text{class}} + \delta C_V^{\text{qm}}$ . An estimate of the statistical error calculated according to ref 41 is given in parentheses.

was calculated using eq 8, by integrating over the density of states,  $\text{DoS}(\nu)$ .

The results are presented in Table 1. Molar heat capacities of the two crystal polymorphs are comparable, as are the results using different force fields. Furthermore, scaling of partial charges causes only a very small and insignificant increase in the heat capacity. Quantum mechanical effects are expected to become important when the quantum mechanical energy  $h\nu$  is comparable to the thermal energy, that is,  $h\nu = k_B T$ . At 298 K, this means wave numbers from around  $100 \text{ cm}^{-1}$ , and higher. Thus, from Figure 4, it is clear that the larger part of the normal mode distribution is residing in the quantum mechanical regime. It is interesting to note that the classical heat capacity at constant volume,  $C_V^{\text{class}}$ , in all cases is very close to the result of Petit and Dulong,  $k_B$  per degree of freedom, which becomes  $648 \text{ J mol}^{-1} \text{ K}^{-1}$  in the present case. Apparently a harmonic model seems a good approximation for the crystal, although there are of course vibrations that are anharmonic, to some extent. The values of  $C_P^{\text{corr}}$  are a little too low compared to the experimental result, which could either be interpreted as a deficiency of the model, or it could be an indication that the simulations are too short to accurately sample the anharmonic contributions to  $C_P$ . To investigate how well these anharmonic contributions were sampled,  $C_P^{\text{class}}$  was plotted against reciprocal simulation time (Figure 6), in order to get a notion of the convergence. Inspection of Figure 6 shows that for the solid, a few nanoseconds of simulation are enough to be able to make a reliable extrapolation to infinite times.

**3.2. Liquid State.** **3.2.1. Liquid Structure.** Liquid [BMIM]-Cl structure was characterized using radial distribution functions (RDFs), and spatial distribution functions (SDFs), cf. Figure 5. Differences between force fields are much larger than between full and scaled charges. Charge scaling only slightly affects the position and height of the peaks, as previously noted by Chaban et al.,<sup>26</sup> and the differences are in fact so small that they would hardly be detectable in a neutron diffraction experiment.

**3.2.2. Heat Capacity of Liquid [BMIM]Cl and Enthalpy of Fusion.** The Molar heat capacity at constant pressure for liquid [BMIM]Cl was calculated at 420 K using the classical value from enthalpy fluctuations from a 50 ns long trajectory where

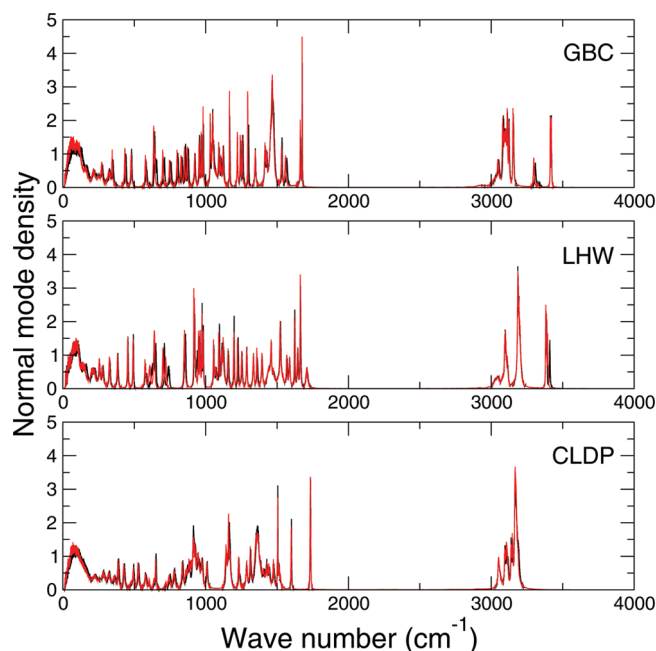


**Figure 4.** Normal mode distribution of the orthorhombic allotrope of crystalline [BMIM]Cl at 298 K. Black curves represent full charges, and red curves show scaled charges. Note that the distributions are normalized to  $3N$  where  $N$  is the number of atoms in one ion pair, which in the present case is equal to 26. The modes at low wavenumbers, (up to approximately  $500 \text{ cm}^{-1}$ ), which contribute most to the heat capacity, are mainly associated with translations and rotations of whole molecules. As one moves to the right in the plots, internal degrees of freedom become more dominating—bond rotations, angle vibrations, and bond vibrations, in that order. Finally, the modes around  $3100 \text{ cm}^{-1}$  originates from vibrations of protons, which give only a negligible contribution to the heat capacity.

the first 5 ns were discarded for equilibration, and with quantum mechanical corrections from the distributions of normal modes (eqs 8 and 9). The results are shown in Table 2. Just as for the solid, the purely classical heat capacities are about twice the experimental values, but when a quantum mechanical correction term is added the situation looks much brighter, and

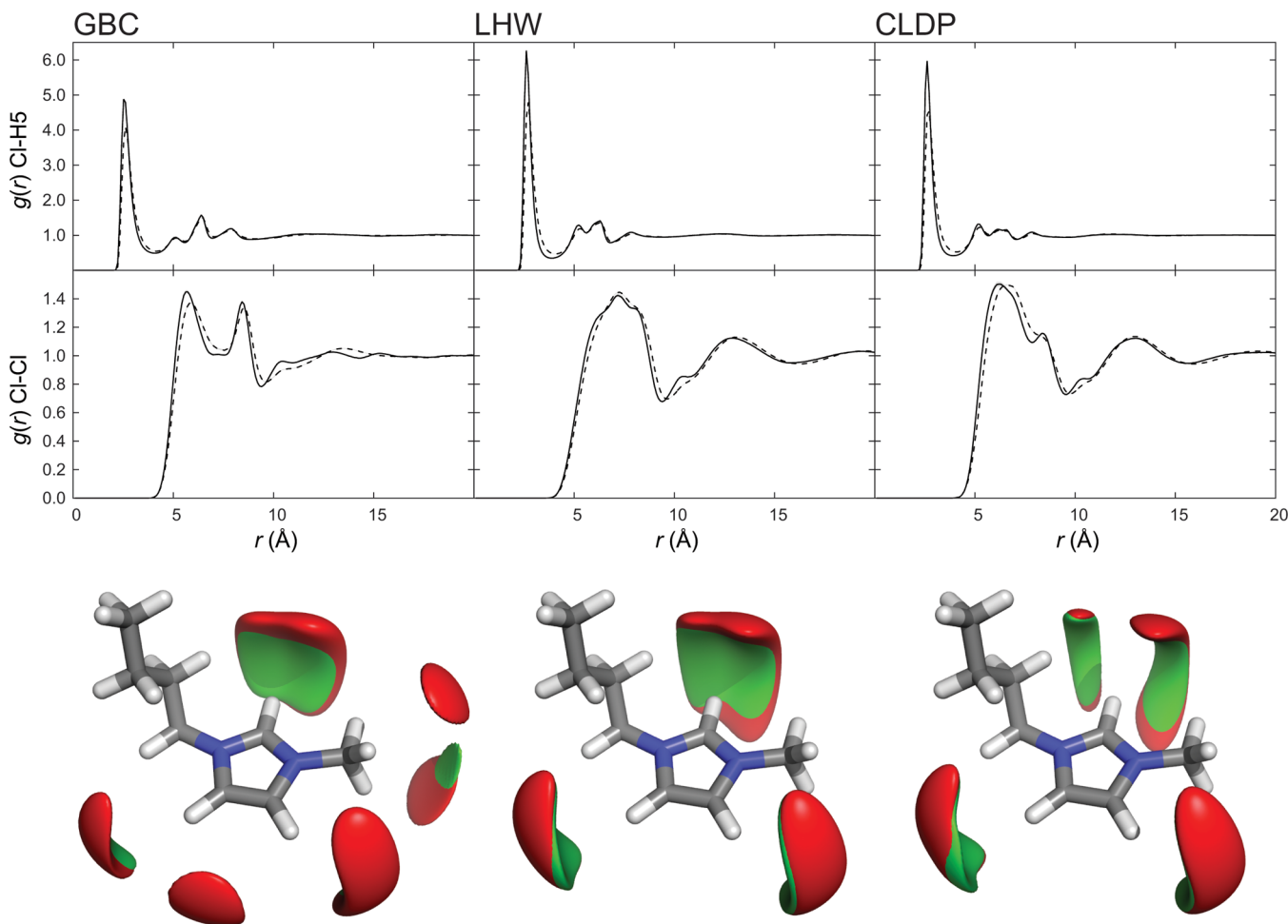


**Figure 5.** Cl–H5 and Cl–Cl radial distribution functions (top, middle) and  $\text{Cl}^-$  distributions around the BMIM $^+$  cation (bottom) for the three different force fields. In the RDFs, solid curves refer to full charges, and dashed curves to scaled charges. For the SDFs, full charges are represented by green surfaces, and scaled charges by red ones.

**Table 2. Molar Heat Capacity of Liquid [BMIM]Cl at 420 K<sup>a</sup>**

	full charges			scaled charges		
	GBC	LHW	CLDP	GBC	LHW	CLDP
$\delta C_V^{\text{qm}}$	-367.2	-389.9	-368.6	-377.6	-401.7	-383.7
$\Delta C$	37.2	33.7	56.2	62.0	61.0	64.7
$C_V^{\text{class}}$	671.0	665.0	677.4	686.0	669.8	678.9
$C_p^{\text{class}}$	708.2	698.7	733.6	748.0	730.8	743.6
$C_p^{\text{corr}}$	341.0 (8.0)	308.8 (8.0)	365.0 (16.8)	370.4 (7.5)	329.1 (7.7)	359.9 (4.0)

<sup>a</sup>The different terms are calculated in the same way as for the solid (see text). An estimate of the statistical error is given in parentheses. The experimental<sup>69</sup> value of  $C_p$  at the present temperature is of 340.37 J mol<sup>-1</sup> K<sup>-1</sup>.

all results end up within 10% of the experimental value<sup>69</sup> of 340.37 J mol<sup>-1</sup> K<sup>-1</sup>.

For all three cases, scaling of partial charges leads to a slightly increased value for the classical  $C_p$ , and at the same time, the correction term becomes larger in magnitude. This leads to that the final value increases with scaled charges for GBC and LHW, while it decreases slightly for the case of CLDP. It appears that, here, scaling mainly affects the normal modes at low frequencies (see Figure 7). This is reasonable since these low frequency motions are mainly associated with large-scale molecular motions, rotations and translations of whole molecules that are more sensitive to nonbonded interactions

than internal vibrations, which are more sensitive to bond and angle potential functions.

Contrary to the solid,  $C_V^{\text{class}}$  of the liquid is significantly higher than  $k_B$  per degree of freedom (648 J mol<sup>-1</sup> K<sup>-1</sup>). This can be understood by the fact that the distribution of normal modes now has a large contribution from anharmonic vibrations, much larger than for the crystal, because the system is a liquid, and also present at a much higher temperature than the solid. These contributions are included in the classical value, but not in the quantum mechanical one, which still is assuming a purely harmonic model. From Figure 6 it is clear that for the solid the fluctuations have converged after only a few nanoseconds but for the liquid the classical heat capacity has not converged until

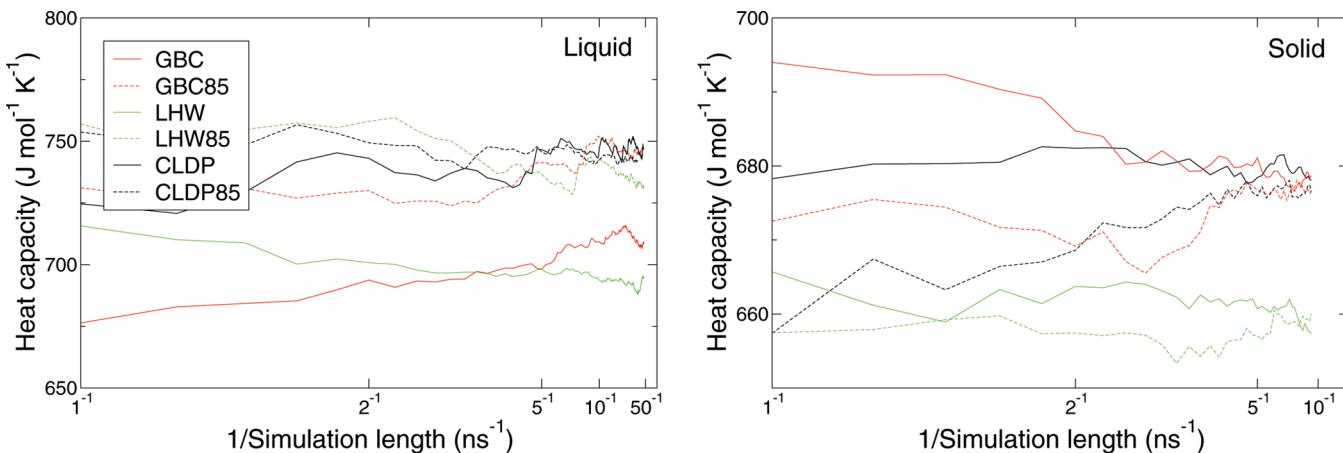


**Figure 6.** Classical molar heat capacity (from enthalpy fluctuations) vs inverse simulation length, for liquid (left) and solid (right) [BMIM]Cl.

after tens of nanoseconds and, in some cases, not even then. This indicates that simulations as long as, at least, several tens of nanoseconds, even at high temperatures (420 K in the present case) are needed to sample all relevant motions of liquid [BMIM]Cl. This also means that the statistical error is potentially larger than what is given in Table 2, and the values of  $C_p$  must therefore be taken as fairly rough estimates. Systems with scaled charges generally exhibit smaller variations than systems with the charges intact, which is a reflection of the higher mobility in these systems, and which leads to more efficient sampling of configurations.

In this context, it is important to remember that the quantum mechanical corrections most likely are overestimated, since  $C_V^{\text{qm}}$  lacks contributions from low frequency motions that are not adequately sampled on a subnanosecond time scale. Still, it is in the low frequency region that the main differences between full and scaled charges are found (see Figure 7).

There is an alternative way of accounting for the anharmonic contributions to the heat capacity that relies on a partitioning of the normal mode spectrum into one harmonic and one diffusive part,<sup>43,44</sup> which has recently been used to calculate thermodynamical properties of water,<sup>44</sup> organic liquids,<sup>41</sup> and

molten salts.<sup>70</sup> This method was tried but deemed insufficient in the present case since it, for computational reasons, must use fairly short ( $\sim 1$  ns) simulations and thus cannot be expected to sample all relevant motions of a highly viscous liquid.

With the  $p\Delta V$  term being negligible, the enthalpy of fusion,  $\Delta_{\text{fus}}H$  of [BMIM]Cl was calculated as the difference in potential energy between the solid (orthorhombic) and the liquid phase, at the experimental melting temperature,  $T_m = 342$  K.<sup>71</sup> Also, energies can be corrected for quantum mechanical effects by adding a correction term calculated from an integral over normal modes:<sup>42</sup>

$$\delta U_{\text{qm}} = \int_0^\infty \left( \frac{h\nu}{2} + \frac{h\nu}{\exp(h\nu) - 1} - k_B T \right) \text{DoS}(\nu) d\nu \quad (10)$$

where the first two terms represent the ground state and the excited states of a quantum mechanical harmonic oscillator, respectively, and the third term is the energy of a harmonic oscillator in the classical limit. The calculated values for  $\Delta_{\text{fus}}H$ , with quantum mechanical corrections, are given in Table 3.

**Table 3. Enthalpy of Fusion from Simulations<sup>a</sup>**

	full charges			scaled charges		
	GBC	LHW	CLDP	GBC	LHW	CLDP
$\Delta_{\text{fus}}H_{\text{class}}$	17.6	29.4	21.3	17.7	26.4	19.8
$\delta\Delta_{\text{fus}}H_{\text{qm}}$	-2.4	-2.0	-1.1	-3.3	-2.1	-2.0
$\Delta_{\text{fus}}H_{\text{corr}}$	15.2	27.4	20.2	14.4	24.3	17.8

<sup>a</sup>The first row is the classical value, obtained directly from simulations ( $\Delta_{\text{fus}}H_{\text{class}} = U^{\text{liq}} - U^{\text{cryst}}$ ), the second row is the quantum mechanical correction calculated using eq 10 ( $\delta\Delta_{\text{fus}}H_{\text{qm}} = \delta U_{\text{qm}}^{\text{liq}} - \delta U_{\text{qm}}^{\text{cryst}}$ ), and the third row is the corrected value ( $\Delta_{\text{fus}}H_{\text{corr}} = \Delta_{\text{fus}}H_{\text{class}} + \delta\Delta_{\text{fus}}H_{\text{qm}}$ ). All values are in kJ mol<sup>-1</sup>. Statistical errors are small, less than 0.1 kJ mol<sup>-1</sup>.

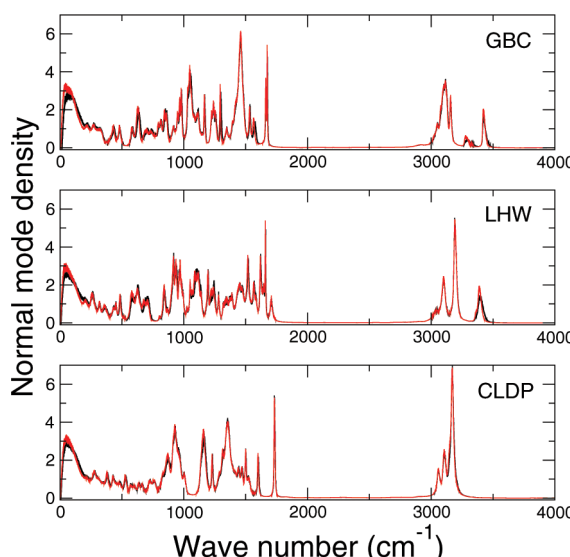


**Figure 7.** Normal mode distributions of liquid [BMIM]Cl at 420 K. Black curves represent full charge, and red curves show scaled charges.

Experimental values of  $\Delta_{\text{fus}}H$  for the orthorhombic allotomorph falls in the range 21.5–25.2 kJ mol<sup>-1</sup>.<sup>71–73</sup> As can be seen from Table 3, the calculated values spread around the experimental ones. Quantum mechanical correction terms take down the values a little bit, but only by 1–3 kJ mol<sup>-1</sup>. Charge scaling has a small effect, but other force field parameters are obviously more important here since differences between the different force fields are much larger.

**3.2.3. Shear Viscosity, Self-Diffusion, and Ionic Conductivity.** The dynamic properties of [BMIM]Cl were

characterized by calculating shear viscosity, self-diffusion coefficients, and ionic conductivity, at 363 K.

The shear viscosity was calculated using the Green–Kubo formalism (see, e.g., Hess<sup>74</sup>):

$$\eta = \frac{V}{k_B T} \int_0^\infty \langle P_{xy}(t_0)P_{xy}(t_0 + t) \rangle_{t_0} dt \quad (11)$$

where  $P_{xy}$  represents the off-diagonal elements of the microscopic pressure tensor. It is evident from Figure 8 and

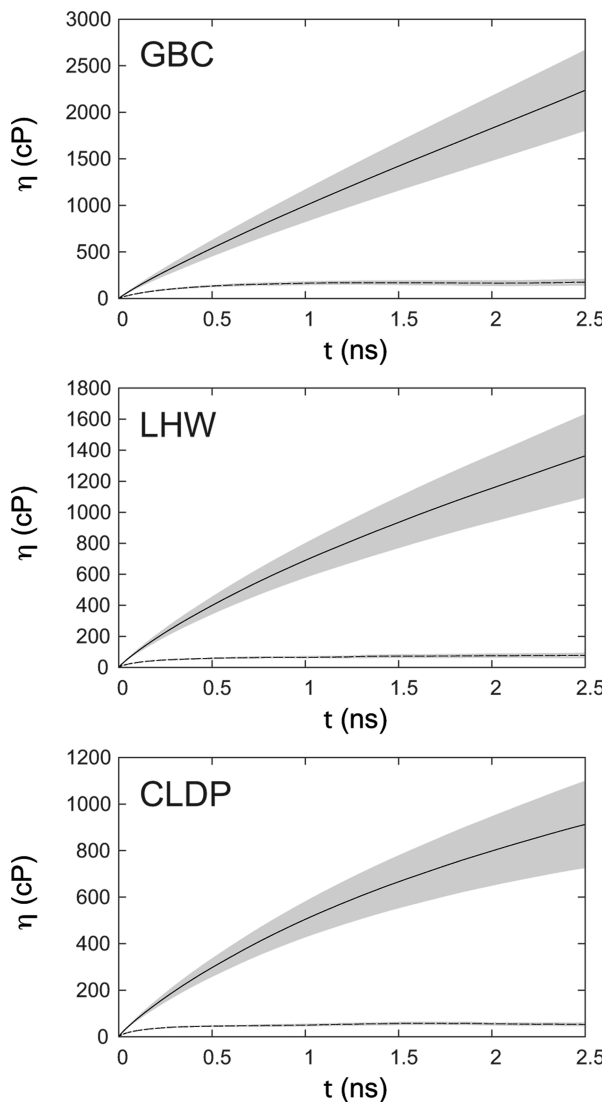


**Figure 8.** Calculated viscosity as a function of the upper limit in the Green–Kubo integral (eq 11) for the three force fields (from top to bottom): GBC, LHW, and CLDP. Solid lines refer to full charges, and dashed lines to scaled charges. The gray area represents the standard error.

Table 4 that the original charge distributions give viscosities that are too high, for all three force fields. Even if the calculations have not converged in the present simulations, it is clear that they are larger than 1000 cP, which make them, at least, an order of magnitude larger than the experimental<sup>75</sup> value of 100 cP, at the present temperature. On the other hand, scaling of the charges to 85% has a dramatic effect on the viscosity. Now the viscosities from all three force fields end up within a factor of 2 of the experimental result. Remembering

that the scale factor of 0.85 used here are somewhat arbitrary, there is clearly room for improvement by fine-tuning of the partial charges to match the experimental viscosity, as in ref 28. However, one has to bear in mind that even if the data for the scaled systems seem converged and the statistical error is fairly small, the results are most likely affected by large uncertainties originating from long correlations in both time and space,<sup>76</sup> which we presently cannot assess. Therefore, such a parametrization might be somewhat problematic, or at least computationally demanding.

There is no experimental value for the self-diffusion coefficient of [BMIM]Cl present in the literature. Tokuda et al.<sup>77</sup> measured self-diffusion for a range of [BMIM]-based ILs which resulted in values in the range  $75\text{--}156 \times 10^{-12} \text{ m}^2/\text{s}$  (see Table 5). Specifically, for ILs having similar viscosity as [BMIM]Cl, the diffusion coefficients were approximately  $130 \times 10^{-12} \text{ m}^2/\text{s}$  and  $94\text{--}143 \times 10^{-12} \text{ m}^2/\text{s}$  for the cation and the anion, respectively. The same research group later performed MD simulations of the same set of ILs using the CLDP force field (with integer charges) and found that diffusion coefficients at 353 K were consistently about 1 order of magnitude smaller than the experimental ones.<sup>78</sup>

There are a few results for the self-diffusion of [BMIM]Cl calculated from MD simulations to be found in literature. Kowsari et al. reported values at 400 K of  $7.2$  and  $7.5 \times 10^{-12} \text{ m}^2/\text{s}$  for cations and anions respectively,<sup>79</sup> and Urahata et al. have reported values of both  $224.8/112.4 \times 10^{-12} \text{ m}^2/\text{s}$  (cations/anions),<sup>80</sup> and later<sup>81</sup>  $14/31 \times 10^{-12} \text{ m}^2/\text{s}$ , also at 400 K. In all three cases, data were based on fairly short (1 ns) simulations, which, in retrospect, seem too short to be reliable.

In the present paper, the translational self-diffusion coefficient was calculated from the slope of the mean square displacement after long times,

$$D = \lim_{t \rightarrow \infty} \frac{1}{6} \frac{d}{dt} \langle [\mathbf{r}(t) - \mathbf{r}(0)]^2 \rangle \quad (12)$$

The translational self-diffusion coefficients are given in Table 4, and the time dependence of the MSDs are shown in Supporting Information Figure S1. It is found that the diffusion coefficients converge quite slowly. For the case of scaled charges, convergence is reached after a few nanoseconds, while it takes about 10 ns for the case of unscaled charges. To achieve satisfactory statistics on these time scales, simulations need to be at least twice as long, in total.

With full charges, self-diffusion coefficients are between  $0.10$  to  $0.93 \times 10^{-12} \text{ m}^2/\text{s}$ , which is more than 2 orders of magnitude smaller than experimental values for [BMIM]<sup>+</sup> based ILs of similar viscosity as [BMIM]Cl.<sup>77</sup> The self-diffusion coefficients for the anions are, consistently, about a factor 1.5 to 2 smaller than for the cations. Using scaled charges, the diffusion coefficients increase dramatically, by a factor 20–32 for the cations, and 35–68 for the anions. This results in that the difference between  $D^+$  and  $D^-$  decreases and actually vanishes within the given errors, but also that the numbers are closer to experimental data for similar ILs, although still a factor 5 to 20 too low. There are large differences between the force fields, with GBC giving the smallest self-diffusion coefficients, followed by LHW and CLDP. This order persists even after charge scaling, but the relative differences decrease. Yeh and Hummer<sup>82</sup> have calculated a correction term to self-diffusion coefficients from MD simulations due to the finite size of the simulation box as  $\delta D = k_B T / 6\pi\eta L$ , where  $L$  is the side length of the cubic box. Here, this correction amounts to approximately

**Table 4.** Diffusion Coefficients ( $D^+$ ,  $D^-$ ) in  $10^{-12} \text{ m s}^{-2}$ , Shear Viscosity ( $\eta$ ) in cP, Ionic Conductivity ( $\sigma$  and  $\sigma_{\text{NE}}$ ) in  $10^{-3} \text{ S m}^{-1}$ , the Factor  $\alpha = \sigma/\sigma_{\text{NE}}$  (See Text), and Hydrodynamic Radius  $R^+$  in Å of the Cation for the Different Force Fields and Charge Distributions at 363 K<sup>a</sup>

	full charges			scaled charges		
	GBC	LHW	CLDP	GBC	LHW	CLDP
$D^+$	0.23 (0.03)	0.93 (0.07)	0.85 (0.14)	7.45 (0.17)	19.0 (0.2)	26.2 (1.7)
$D^-$	0.098 (0.02)	0.53 (0.09)	0.53 (0.15)	6.64 (0.79)	18.5 (0.7)	28.2 (1.1)
$\eta$	2216 (430)	1353 (267)	907 (185)	168 (28)	75 (13)	56 (6.4)
$\sigma$	1.85 (0.9)	13.6 (3.7)	14.4 (5.3)	112 (41)	436 (109)	537 (179)
$\sigma_{\text{NE}}$	6.0 (0.7)	27.0 (2.0)	25.7 (3.8)	178 (14)	483 (13)	701 (36)
$\alpha$	0.31 (0.15)	0.50 (0.14)	0.56 (0.23)	0.62 (0.24)	0.90 (0.23)	0.77 (0.26)
$R^+$	7.8 (2.0)	3.2 (0.6)	5.1 (1.4)	3.2 (0.6)	2.9 (0.5)	2.7 (0.3)

<sup>a</sup>Here,  $D^+$  is the diffusion coefficient of the cation, and  $D^-$  is the diffusion coefficient of the anion. The conductivity  $\sigma$  is calculated from Green–Kubo integrals, while  $\sigma_{\text{NE}}$  are calculated using the Nernst–Einstein approach. The viscosity for the case of full charges is given as the average over the last 50 ps in Figure 8. This means that values for  $\eta$  and  $R^+$ , in this case, are not properly converged. For scaled charges, the averaging is performed over the last nanosecond. Estimated standard errors are given in parenthesis.

**Table 5.** Experimental<sup>77</sup> Viscosity (in cP), Self-Diffusion (in  $10^{-12} \text{ m}^2 \text{ s}^{-1}$ ), and Conductivity Data (in  $\text{S m}^{-1}$ ) at 363 K for [BMIM]<sup>+</sup>-Based ILs with Different Anions

anion	$\eta$	$D^+$	$D^-$	$\sigma$	$\sigma/\sigma_{\text{NE}}$
$\text{PF}_6^-$	186	93	75	1.6	0.68
$(\text{C}_2\text{F}_5\text{SO}_2)_2\text{N}^-$	110	126	94	1.2	0.60
$\text{CF}_3\text{SO}_3^-$	106	127	113	1.9	0.60
$\text{BF}_4^-$	105	134	143	2.7	0.64
$\text{CF}_3\text{CO}_2^-$	76	151	136	2.1	0.50
$(\text{CF}_3\text{SO}_2)_2\text{N}^-$	76	182	156	2.0	0.58

10%, for both the scaled and the unscaled case. This is surely not negligible in a general sense, but given the magnitude of other errors present, a more detailed discussion is not necessary in the present case.

The self-diffusion coefficient and the viscosity is related through the Stokes–Einstein relation, which can be written

$$D\eta = \frac{k_B T}{c\pi R} \quad (13)$$

where  $R$  is the hydrodynamic radius of the molecule, and  $c$  is six under ideal hydrodynamic conditions, but closer to four for ILs.<sup>83</sup> Using the experimental data,<sup>77</sup> it is possible to calculate an experimental hydrodynamic radius of [BMIM]<sup>+</sup> to  $R^+ = 0.3 \text{ \AA}$  (see Figure 9). This is certainly very small, much smaller than the real molecular radii. It might be interpreted as the ions diffusing faster than what is expected from classical hydrodynamics at this viscosity and temperature. However, simulations give radii that are about 1 order of magnitude larger (see Table 4), and moreover essentially unaffected by charge-scaling. This suggests that for [BMIM]Cl it is not possible to achieve agreement with experimental data for both viscosity and self-diffusion coefficients simultaneously using charge-scaling only. However, Martinelli et al.<sup>83</sup> measured  $R^+$  for the [BMIM]<sup>+</sup> cation in [BMIM][TFSI] to  $R^+ = 2.5 \text{ \AA}$ , at 313 K. So, there seems to be a nontrivial dependence also on the anion. Apparently, this remains an open issue due to the lack of experimental self-diffusion data for this particular system.

Assuming that ions move independently of each other, the static ionic conductivity can be related to the self-diffusion of ions through the Nernst–Einstein equation:

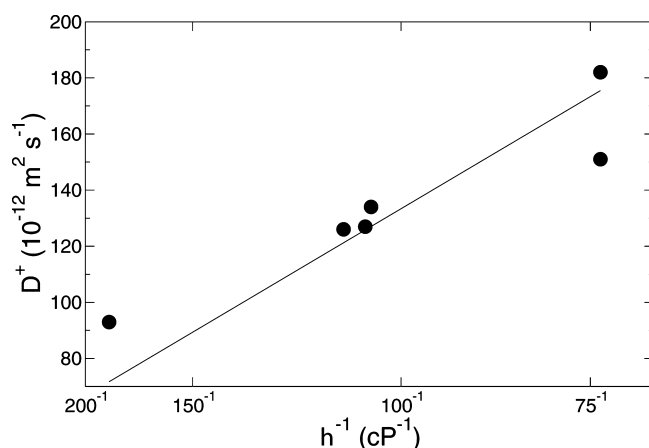


**Figure 9.** Self-diffusion coefficient vs inverse viscosity. The slope corresponds to a hydrodynamic radius of 0.3 Å. Data from Tokuda et al.<sup>77</sup>

$$\begin{aligned} \sigma_{\text{NE}} &= \lim_{t \rightarrow \infty} \frac{e^2}{6tVk_B T} \sum_i^n z_i^2 \langle [\mathbf{r}_i(t) - \mathbf{r}_i(0)]^2 \rangle \\ &= \frac{e^2}{Vk_B T} (n^+ D^+ + n^- D^-) \end{aligned} \quad (14)$$

where  $e$  is the electron charge,  $z_i$  is the charge of ion  $i$  in electrons, and  $\mathbf{r}_i(t)$  is the position of ion  $i$  at time  $t$ . However, since the motions of cations and anions are highly correlated, it is better to consider the Einstein–Helfand approach, in which the static conductivity is obtained from the slope of the mean-squared displacement of the collective translational dipole moment<sup>84</sup>

$$\sigma = \frac{1}{6Vk_B T} \lim_{t \rightarrow \infty} \frac{d}{dt} \langle [\mathbf{M}_j(t) - \mathbf{M}_j(0)]^2 \rangle \quad (15)$$

Here

$$\mathbf{M}_j(t) = \sum_i z_i \cdot \mathbf{r}_i(t) \quad (16)$$

using the same notation as above. The values obtained using both methods mentioned above are given in Table 4, and the result using the latter is shown in Figure 10. There are no experimental values for the conductivity of [BMIM]Cl present in literature. Both Tokuda et al.<sup>77</sup> and Zech and co-workers<sup>85</sup>

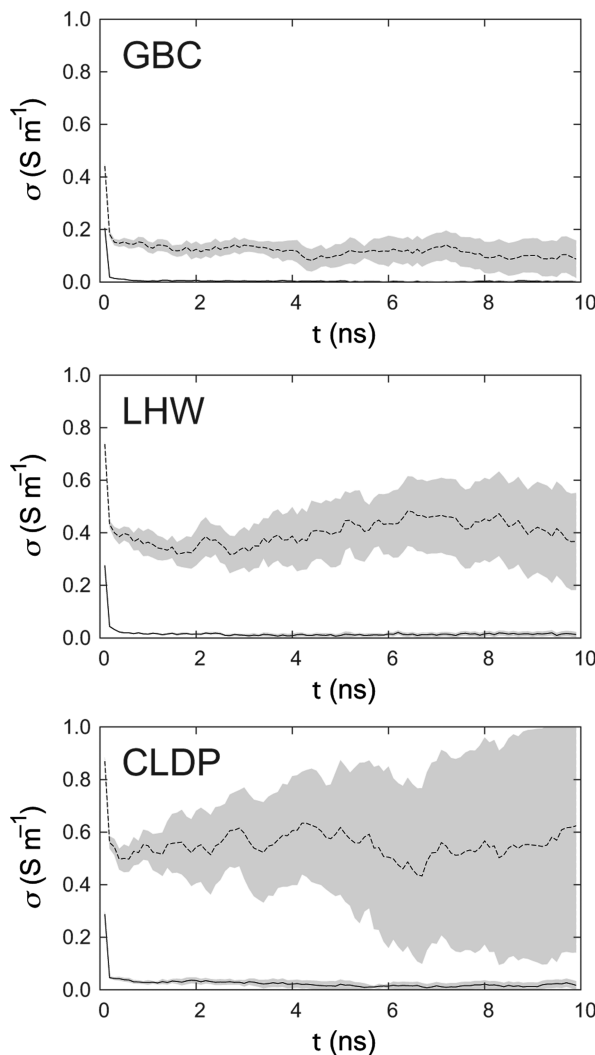


**Figure 10.** Calculated ionic conductivity from eq 15, as a function of time, using full (solid lines) and scaled (dashed) charges for (from top to bottom) GBC, LHW, and CLDP. Gray areas represent the standard error.

measured static conductivity for ILs comprised of  $[\text{BMIM}]^+$  in combination with several other anions, and obtained results in the range  $1.6$  to  $5 \text{ S m}^{-1}$  at the present temperature, with most values being close to  $2$  (see Table 5). Furthermore, Vila et al.<sup>86</sup> obtained a value of  $2.5 \text{ S m}^{-1}$  for  $[\text{EMIM}]^+\text{Cl}^-$  at this temperature, which makes an estimate of  $\sigma \approx 2 \text{ S m}^{-1}$  for  $[\text{BMIM}]^+\text{Cl}^-$  at  $363 \text{ K}$  a reasonable guess. Obviously, values calculated with full charges are much too low compared to this estimate. Scaling the charges improves the situation, but calculated values are still a factor 5 to 20 too low. Just as for the self-diffusion, it seems as if the charges would have to be scaled by a factor smaller than  $0.85$  to achieve better agreement with the real system, at the expense of worse agreement for the viscosity.

When calculating  $\sigma$  from simulations with scaled charges, one has to choose whether  $z_i$  in eq 16 is really  $\pm 0.85$ , or if, since charge scaling can be viewed as a way to model the effects of polarization only,  $z_i = \pm 1$  should be used instead. Here, we report the values using the scaled charges, but we note that to transform them to the integer case,  $\sigma$  needs to be scaled by a factor  $1/0.85^2 = 1.38$ .

It is sometimes useful to introduce the ratio  $\alpha = \sigma/\sigma_{\text{NE}}$  as a measure of the degree of uncorrelated motions.<sup>16,77</sup> Tokuda et al.<sup>77</sup> combined their conductivity measurements with conductivities calculated from NMR using the Nernst–Einstein equation, which resulted in values in the range  $0.50$ – $0.68$  at  $363 \text{ K}$ . Borodin<sup>16</sup> has calculated  $\alpha$  from simulations using a polarizable force field for a number of ILs, which resulted in  $\alpha = 0.58$  to  $0.85$ . In the present paper,  $\alpha$  was calculated using eqs 14 and 15, which resulted in values for  $\alpha$  between  $0.31$  to  $0.90$  (see Table 4). Generally, scaling of partial charges results in an increased  $\alpha$ , meaning that the motions of cations and anions become less correlated, which also makes sense intuitively.

Uniform scaling of partial charges dramatically improves transport properties of  $[\text{BMIM}]^+\text{Cl}^-$ . It seems however that full agreement cannot be obtained for all properties investigated here, simultaneously, using a single scale factor. However, as Dommert and Holm<sup>30</sup> have shown for the case of  $[\text{MMIM}]^+\text{Cl}^-$ , it might be possible to obtain better agreement for a broader range of properties using a more careful assignment of partial charges that is based on the polarization state of the bulk liquid.

**3.3. Binary System  $[\text{BMIM}]^+\text{Cl}^-$ /Ethanol.** A large part of the current interest for ILs comes from their capabilities as solvents for biomass. For that reason, several simulation studies focused on IL/carbohydrate interactions. Unfortunately, available experimental data for IL/carbohydrate systems are scarce, and therefore, validation of molecular force fields for these systems becomes problematic. On the other hand, the availability of experimental data for combinations with other solutes (e.g., alcohols) is much better. Specifically, the binary mixture of  $[\text{BMIM}]^+\text{Cl}^-$  and ethanol has been experimentally characterized with regard to a few thermodynamic properties, densities,<sup>87</sup> and vapor pressure data.<sup>88</sup> In the present study, ethanol was therefore chosen as a model for polar solutes in general, with the assumption that the results are transferable to carbohydrates, at least in a qualitative sense.

**3.3.1. Activity Coefficients.** ILs have negligible vapor pressure under normal pressure and temperature conditions. Previously, excess enthalpies<sup>89</sup> and excess volumes<sup>90</sup> as a function of composition for IL/ethanol systems, as well as excess chemical potentials for a number of small solutes,<sup>91</sup> have been reported from MD simulations, without quantitative experimental validation. Qualitatively, they all give negative excess quantities for the mixtures, suggesting that the chemical potential of an alcohol molecule is lower in the IL than in the pure state.

Calvar and co-workers<sup>88</sup> have reported vapor–liquid equilibrium (VLE) data for the binary mixtures of  $[\text{BMIM}]^+\text{Cl}^-$ /ethanol at atmospheric pressure. They give boiling point temperatures,  $T_B$ , for the IL/ethanol binary mixture as a function of composition, with the mole fraction of ethanol,  $x_1$ , ranging from  $0.5$  to  $1$ . From this, the activity coefficient (at  $T_B$ ) can be calculated using Raoult's law,

$$P = x_1 P_1^* \gamma_1 + (1 - x_1) P_2^* \gamma_2 \quad (17)$$

where  $P$  is the system pressure (1 atm in present case),  $x_1$  is the mole fraction of ethanol,  $\gamma_1$  and  $\gamma_2$  are the activity coefficients of ethanol and IL respectively, and  $P_1^*$  and  $P_2^*$  are the respective partial vapor pressures of the pure phase, at  $T_B$ . Using  $P_2^* = 0$ , and with  $P_1^*$  from literature,  $\gamma_1$  can be calculated as a function of  $x_1$ . Calvar et al. then use the Non-Random Two Liquid model (NRTL)<sup>92</sup> to connect their data with thermodynamics. Specifically, the excess free energy was expressed as a function

of composition. It is important to remember that NRTL is an empirical model based on pairwise molecular interaction parameters, but for the case of ionic liquids, it has been shown to provide excellent agreement with experimental data, superior to other empirical models of the same kind.<sup>93,94</sup>

The activity coefficient is related to the difference in chemical potential,  $\Delta\mu$ , of a solute molecule between the mixture ( $\mu$ ) and some reference state ( $\mu^0$ ), which in the present case is pure liquid ethanol, through

$$\mu = \mu^0 + RT \ln(x_1 \gamma_1) \quad \text{or} \quad \frac{\Delta\mu}{RT} = \ln(x_1 \gamma_1) \quad (18)$$

From the perspective of MD simulations, it is better to express  $\gamma_1$  in terms of the excess (or residual) chemical potential,  $\mu_E$ , instead. The excess chemical potential is the difference in chemical potential between the solute in solution and the solute ideal gas (which conveniently removes the explicit  $x_1$  dependence in eq 18) and can be calculated from MD using free energy perturbation methods or, as in the present case, by thermodynamic integration. Expressed in  $\mu_E$ , eq 18 becomes<sup>95,96</sup>

$$\ln \gamma_1 = \frac{(\mu_E - \mu_E^0)}{RT} = \frac{\Delta\mu_E}{RT} \quad (19)$$

One difficulty that arises when one wants to compare simulation results with experimental VLE data is that the temperature is not constant in the experiments. Since  $\gamma_1$  is given at the boiling point for each composition, simulations must be performed at different temperatures as well for the comparison to be meaningful. However, one way to overcome this is to use the reported NRTL parameters ( $a$ ,  $\Delta g_{12}$ , and  $\Delta g_{21}$ , from Table 4 in ref 88) and back-calculate the activity coefficients at constant temperature within the NRTL theory:

$$\ln \gamma_1 = x_2^2 \left[ \frac{\tau_{21} G_{21}^2}{(x_1 + x_2 G_{21})^2} + \frac{\tau_{11} G_{12}^2}{(x_2 + x_1 G_{12})^2} \right] \quad (20)$$

where  $x_2 = 1 - x_1$ ,  $\tau_{ij} = \Delta g_{ij}/RT$  and  $G_{ij} = \exp(-a\tau_{ij})$ . The resulting  $\gamma_1$ , which is now only a function of  $x_1$  for a fixed value of  $T$ , can be directly compared to eq 19, with  $\Delta\mu_E$  from simulations.

Activity coefficients of ethanol in [BMIM]Cl for the CLDP/OPLS-AA force field were calculated using eq 19. These are plotted in Figure 11 together with extrapolated experimental values from VLE data using NRTL theory (eq 20). From Figure 11 it can be seen that the activity coefficient of ethanol,  $\gamma_1$  is always smaller than one, implying a negative deviation from Raoult's law. It is always *more* favorable for an ethanol molecule to dissolve in the mixture than in the pure substance. That simulations and NRTL theory give the same answer at  $x_1 = 1$  is trivial, but more interestingly they also agree at high dilution,  $x_1 \leq 0.4$ . For increasing  $x_1$  however, the MD curve falls below the NRTL curve. On the other hand, using scaled charges, the MD curve follows the NRTL curve rather well for high  $x_1$  values, but at lower concentrations, it deviates substantially from the NRTL curve and at infinite dilution it is off by more than a factor of 2.

Similar results are obtained for the other two force fields as well (see Table 6). With scaled charges,  $-\ln \gamma_1$  at infinite dilution is substantially reduced compared to full charges. For the GBC model, this means that  $-\ln \gamma_1$ , being on the small side already with charges intact, becomes almost zero when the charges are reduced. For LHW on the other hand, reducing the

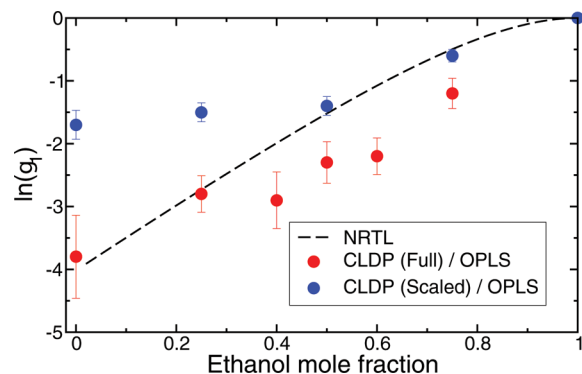


**Figure 11.** Activities of binary systems [BMIM]Cl/EtOH for the CLDP/OPLS-AA FF using both full (red) and scaled (blue) partial charges, as a function of ethanol mole fraction. The dashed curve is the NRTL result, calculated from eq 20 with parameters from ref 88. Error bars show statistical errors from the BAR<sup>63</sup> analysis.

charges actually brings  $-\ln \gamma_1$  closer to the NRTL result. Since it is likely that the negative deviation from Raoult's law is caused by the strong electrostatic interaction in the IL, it is not surprising that reduced partial charges gives an activity closer to one. What is perhaps more surprising is the level of agreement between NRTL theory and MD.

Berens et al.<sup>42</sup> have given expressions for quantum corrections to classical free energies, similar to that for the heat capacity (eq 8). In the light of the results obtained for  $C_p$  of pure [BMIM]Cl, it is entirely possible that such a correction would be non-negligible also for the mixture. A large part of the correction would certainly cancel out when calculating the difference ( $\Delta\mu_E$ ), but to what extent it would still contribute, or the sign of the contribution, cannot be assessed in any trivial way. The simulations involved to calculate the corrections are fairly cumbersome and were not undertaken for the present paper.

The ethanol models used in the simulations are very similar. Since electrostatics dominates the interactions, it is reasonable to analyze the dipole moments of the ethanol molecules. Averaged over 5 ns simulations, they are 2.4 D for CHARMM and OPLS, and 2.2 D for the AMBER model. Based on this, one would anticipate that the AMBER ethanol would give an activity closer to one than the other two models. Since it is the other way around, the choice of IL model is, evidently, more crucial here.

Given that the NRTL curve is based on measurements at  $x_1 \geq 0.5$  only, it is tempting to conclude that it is more reliable at high [BMIM]Cl contents, where scaled charges give the best fit. However, the picture is more complex than that. It is possible to rationalize some of these results by examining the density, and put it in relation to the electrostatic energy density. Kobrak and Li<sup>97,98</sup> give an expression for the electrostatic energy between a small dipole and a surrounding ionic liquid medium:

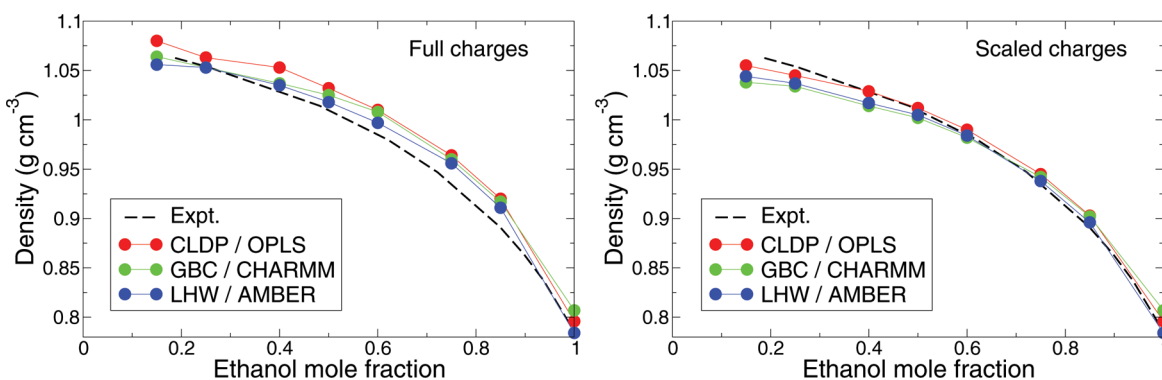
$$E = \frac{p}{2\epsilon_0} A \sin|\phi| \quad (21)$$

where  $p$  is the solute dipole moment,  $\epsilon_0$  the permittivity of free space, and  $A \sin |\phi|$  is a factor that describes the charge density around the solute. The amplitude  $A$  depends linearly on the ionic charge, and further has an unspecified direct relationship with the solvent number density. Thus, the model predicts, quite intuitively, that an increased density will lead to more electrostatic energy per solute molecule, and consequently a

**Table 6.** Calculated Chemical Potentials at  $T = 350$  K of Ethanol in the Pure State ( $\mu^0$ ) and in [BMIM]Cl at High Dilution ( $\mu^\infty$ ) Relative the Vapor in Units of  $k_B T$ , and the Resulting  $-\ln \gamma_1$  at High Dilution<sup>a</sup>

	full charges				scaled charges			
	$\mu^0$	$\mu^\infty$	$-\ln \gamma_1$	$\rho_{IL}$	$\mu^0$	$\mu^\infty$	$-\ln \gamma_1$	$\rho_{IL}$
CLDP	5.9	9.7	3.8	1.062	5.9	7.6	1.7	1.039
GBC	6.5	9.1	2.6	1.047	6.5	7.0	0.5	1.024
LHW	6.6	12.0	5.4	1.048	6.6	9.6	3.0	1.028
NRTL/expt.			4.0	1.054				

<sup>a</sup>The NRTL value is based on experimental data and fitted NRTL parameters from ref 88. Included are also calculated and experimental<sup>99</sup> densities (in g cm<sup>-3</sup>) of the pure IL at this temperature.

**Figure 12.** Calculated and experimental<sup>100</sup> densities of the binary system [BMIM]Cl/ethanol at 298 K as a function of ethanol mole fraction. The curves do not start at zero ethanol content since the pure IL is not a liquid at this temperature.

lower activity. As seen from Table 6, as the charges are reduced to 85%, the chemical potential of ethanol in the IL decreases, but rather by 20–23% than the expected 15%. This is likely a consequence of that the system density at high dilution decreases too, for all models (see Table 6).

Calculated densities at 298 K as a function of ethanol mole fraction ( $x_1$ ) of the IL/ethanol systems are shown in Figure 12 together with experimental values from Calvar et al.<sup>87</sup> As can be seen, the densities from simulations using full charges are close to the experimental value at low  $x_1$ , with the exception of CLDP which is a little higher, but at higher  $x_1$ , all calculated curves lie above the experimental one. Using scaled charges on the other hand, the calculated density curves lie on top of the experimental one for high values of  $x_1$ , but drop below the experimental curve at low  $x_1$ . Thus, the calculated density curves correlate with the calculated activities in Figure 11; at high dilution, full charges give better agreement with both experimental densities and activities, while scaled charges are better at higher ethanol content. These results are actually quite counterintuitive. Since charge reduction is meant to compensate for the lack of polarizability, one would think that reduced charges would perform better at high IL concentrations where polarization effects are likely to become more important. The fact that it is the other way around is probably a consequence of that charge reduction, while being a viable approach for the pure IL, is not the best option for mixtures. To describe interactions between the ILs and polar solutes satisfactorily, an explicit polarizability must likely be included in the model, in some way.

#### 4. CONCLUSIONS

In the present study, three widely used molecular force fields for ionic liquids were used to simulate both crystalline and liquid [BMIM]Cl, and its binary mixtures with ethanol. To

investigate the effect of uniformly scaled partial charges, the simulations were performed both with the original integer charges ( $\pm 1$  on each ion), and with the partial charges scaled to 85%.

For crystalline [BMIM]Cl at 298 K, the CLDP force field gives the best match to the experimental crystal structure for the monoclinic polymorph, while LHW performed best for the orthorhombic polymorph, as judged from the RMSDs of the time-averaged lattice parameters. Uniform scaling of partial charges was found to significantly increase the RMSD in all cases, except for the orthorhombic structure with LHW, which remained unaffected. The molar heat capacity at constant pressure,  $C_p$ , was insensitive both to choice of force field and scaling of partial charges. Molar heat capacities calculated from (classical) energy fluctuations with a quantum mechanical correction based on the distribution of normal modes were found to be in reasonable agreement with experimental numbers.

Liquid [BMIM]Cl was investigated by its thermodynamical, structural, and dynamical properties. The liquid structure of [BMIM]Cl is not significantly affected by charge scaling, as judged by radial and spatial distribution functions (RDFs and SDFs). There are larger variations between the force fields, than between charge distributions within the same force field.

The QM-corrected molar heat capacity at constant volume was in fair agreement with experimental data. For GBC and LHW, it was too low with full charges, but too high after charge reduction. For CLDP, it was too high with full charges, whereas it remained essentially unaffected by charge scaling. Without the quantum mechanical correction, values for the molar heat capacity were around twice the experimental number. Also, the QM-corrected calculated heats of fusion were close to the experimental values. Charge scaling only had a minor effect on  $\Delta_{\text{fus}}H$ , much smaller than the differences between the force fields.

The dynamical properties (viscosity, self-diffusion and conductivity) are the ones that are most affected by charge reduction, a fact of which there are numerous accounts in the literature. With full charges, everything moves too slowly, leading to too high viscosities and too low translational self-diffusion coefficients and static ionic conductivity. Generally, the deviations from experimental data are orders of magnitude in size. For the present IL, scaling of the charges by a factor 0.85 leads to viscosities that are within a factor two of the experimental number of 100 cP, but with both self-diffusion and ionic conductivity remaining a factor 5 to 20 too low. Apparently, uniform scaling of partial charges cannot provide agreement between simulations and experiments for all three properties at the same time. Moreover, one has to remember that charge scaling also affects internal interactions of the imidazolium cation. While this surely has very little effect on the structure of the imidazole ring, it may very well affect both the flexibility and equilibrium conformation of the alkyl side-chain, which in turn could have a direct influence of the overall viscosity of the liquid. Such problems can be avoided if the assignment of partial charges is done already at the initial parametrization stage.<sup>30</sup>

The binary mixture [BMIM]Cl/ethanol was studied at two different temperatures, 298 and 350 K, at several ethanol mole fractions from  $x_1 = 0$  to  $x_1 = 1$ . The activity coefficient of ethanol,  $\gamma_1$ , was calculated and compared to experimental VLE data,<sup>88</sup> which was extrapolated to constant temperature using NRTL theory. Ethanol activity at infinite dilution was in fair agreement with the NRTL value, and always less than unity, for all three force fields investigated. A reduction of partial charges to 85% lead to an increase of the chemical potential of ethanol in [BMIM]Cl by  $2k_B T$ , thus bringing  $\gamma_1$  closer to one. This is an effect of both weaker electrostatic potentials and a reduced density.

Although simulations with the unmodified CLDP force field could reproduce ethanol activity from VLE data at high dilution, it failed to do so for higher ethanol contents. However, when reduced charges were used, activities at high  $x_1$  were in good agreement with VLE data, whereas they were too close to one at low  $x_1$ . This result correlated well with the calculated densities, which were too high at high  $x_1$  using unscaled charges, and too low at low  $x_1$  when the charges were reduced. In this respect, the system density of the binary mixture is a good indicator also for the chemical potential; if the chemical potential is to be reproduced across the whole range of compositions, then, seemingly, the density has to be reproduced as well. To achieve this, however, there seems to be a need for a model that can account for the change in polarization as the composition is varied. The fact that the physical properties depend so strongly on the state of polarization unfortunately indicates that any model that uses static charges is likely to have to be reparametrized for each new composition. This makes a model that incorporates explicit polarizability,<sup>12,16,101</sup> for both ILs and solutes, desirable.

## ASSOCIATED CONTENT

### Supporting Information

Relative deviation of all crystal lattice parameters from their corresponding experimental value; the time dependence of the Mean Square Displacements; convergence of self-diffusion coefficients for liquid [BMIM]Cl. This material is available free of charge via the Internet at <http://pubs.acs.org>.

## AUTHOR INFORMATION

### Corresponding Author

\*Email: jacke@kth.se

### Present Address

<sup>†</sup>Department of Biomedical Engineering, Oregon Health and Science University, Oregon 97239, U.S.A.

### Author Contributions

<sup>†</sup>M.C. and R.P. contributed equally to this work.

### Notes

The authors declare no competing financial interest.

## ACKNOWLEDGMENTS

This work was funded by grants from the Swedish Research Council and the Stockholm University Academic Initiative. Computing resources were kindly provided by the PDC Center for High Performance Computing, Stockholm, Sweden, and the Extreme Science and Engineering Discovery Environment (XSEDE), which is supported by National Science Foundation grant No. OCI-1053575

## REFERENCES

- (1) Hallett, J. P.; Welton, T. *Chem. Rev.* **2011**, *111*, 3508–3576.
- (2) Swatloski, R. P.; Spear, S. K.; Holbrey, J. D.; Rogers, R. D. *J. Am. Chem. Soc.* **2002**, *124*, 4974–4975.
- (3) Zakerzewska, M. E.; Bogel-Lukasik, E.; Bogel-Lukasik, R. *Energy Fuels* **2010**, *24*, 737–745.
- (4) Schrems, M.; Brandt, A.; Welton, T.; Liebner, F.; Rosenau, T.; Potthast, A. *Holtzforschung* **2011**, *65*, 527–533.
- (5) Sun, N.; Rodríguez, H.; Rahman, M.; Rogers, R. D. *Chem. Commun.* **2011**, *47*, 1405–1421.
- (6) Copley, J. R. D.; Rahman, A. *Phys. Rev. A* **1976**, *13*, 2276–2286.
- (7) de Andrade, J.; Böes, E. S.; Stassen, H. *J. Phys. Chem. B* **2002**, *106*, 13344–13351.
- (8) Jorgensen, W. L.; Maxwell, D. S.; Tirado-Rives, J. *J. Am. Chem. Soc.* **1996**, *118*, 11225–11236.
- (9) Cornell, W. D.; Cieplak, P.; Bayly, C. I.; Gould, I. R.; Merz, K. M.; Ferguson, D. M.; Spellmeyer, D. C.; Fox, T.; Caldwell, J. W.; Kollman, P. A. *J. Am. Chem. Soc.* **1995**, *117*, 5179–5197.
- (10) Canongia Lopes, J. N.; Deschamps, J.; Pádua, A. A. H. *J. Phys. Chem. B* **2004**, *108*, 2038–2047.
- (11) Liu, Z.; Huang, S.; Wang, W. *J. Phys. Chem. B* **2004**, *108*, 12978–12989.
- (12) Dommert, F.; Wendler, K.; Berger, R.; Delle Site, L.; Holm, C. *ChemPhysChem* **2012**, *13*, 1625–1637.
- (13) Hunt, P. A. *Mol. Sim.* **2006**, *32*, 1–10.
- (14) Youngs, T. G. A.; Hardacre, C. *ChemPhysChem* **2008**, *9*, 1548–1558.
- (15) Yan, T.; Burnham, C. J.; Del Pópolo, M. G.; Voth, G. A. *J. Phys. Chem. B* **2004**, *108*, 11877–11881.
- (16) Borodin, O. *J. Phys. Chem. B* **2009**, *113*, 11463–11478.
- (17) Köddermann, T.; Paschek, D.; Ludwig, R. *ChemPhysChem* **2007**, *8*, 2464–2470.
- (18) Köddermann, T.; Paschek, D.; Ludwig, R. *ChemPhysChem* **2008**, *9*, 549–555.
- (19) Köddermann, T.; Ludwig, R.; Paschek, D. *ChemPhysChem* **2008**, *9*, 1851–1858.
- (20) Roth, C.; Appelhagen, A.; Jobst, N.; Ludwig, R. *ChemPhysChem* **2012**, *13*, 1708–1717.
- (21) Vatamanu, J.; Borodin, O.; Smith, G. D. *J. Am. Chem. Soc.* **2010**, *132*, 14825–14833.
- (22) Vatamanu, J.; Borodin, O.; Smith, G. D. *J. Phys. Chem. B* **2011**, *115*, 3073–3084.
- (23) Vatamanu, J.; Borodin, O.; Bedrov, D.; Smith, G. D. *J. Phys. Chem. C* **2012**, *116*, 7940–7951.
- (24) Bühl, M.; Chaumont, A.; Schurhammer, R.; Wipff, G. *J. Phys. Chem. B* **2005**, *109*, 18591–18599.

- (25) Bowron, D. T.; D'Agostino, C.; Gladden, L. F.; Hardacre, C.; Holbrey, J. D.; Lagunas, M. C.; McGregor, J.; Mantle, M. D.; Mullan, C. L.; Youngs, T. G. *A. J. Phys. Chem. B* **2010**, *114*, 7760–7768.
- (26) Chaban, V. V.; Voroshlyova, I. V.; Kalugin, O. N. *Phys. Chem. Chem. Phys.* **2011**, *13*, 7910–7920.
- (27) Schmidt, J.; Krekeler, C.; Dommert, F.; Zhao, Y.; Berger, R.; Delle Site, L.; Holm, C. *J. Phys. Chem. B* **2010**, *114*, 6150–6155.
- (28) Chaban, V. *Phys. Chem. Chem. Phys.* **2011**, *13*, 16055–16062.
- (29) Wendler, K.; Dommert, F.; Zhao, Y. Y.; Berger, R.; Holm, C.; Delle Site, L. *Faraday Discuss.* **2012**, *154*, 111–132.
- (30) Dommert, F.; Holm, C. *Phys. Chem. Chem. Phys.* **2013**, *15*, 2037–2049.
- (31) Mondal, A.; Balasubramian, S. *J. Phys. Chem. B* **2014**, *118*, 3409–3422.
- (32) Leontyev, I.; Stuchebrukhov, A. *Phys. Chem. Chem. Phys.* **2011**, *13*, 2613–2626.
- (33) Liu, Z.; Remsing, R. C.; Moore, P. B.; Moyna, G. In *Ionic Liquids IV*; Brennecke, J., et al., Eds.; ACS Symposium Series; American Chemical Society: Washington, DC, 2007; pp 335–349.
- (34) Petrik, I. G.; Remsing, R. C.; Liu, Z.; O'Brien, B. B.; Moyna, G. In *Ionic Liquids: From Knowledge to Application*; Plechko, N., et al., Eds.; ACS Symposium Series; American Chemical Society: Washington, DC, 2009; pp 75–91.
- (35) Youngs, T. G. A.; Holbrey, J. D.; Mullan, C. L.; Norman, S. E.; Lagunas, M. C.; D'Agostino, C.; Mantle, M. D.; Gladden, L. F.; Bowron, D. T.; Hardacre, C. *Chem. Sci.* **2011**, *2*, 1594–1605.
- (36) Zhao, Y.; Liu, X.; Wang, J.; Zhang, S. *ChemPhysChem* **2012**, *13*, 3126–3133.
- (37) Zhao, Y.; Liu, X.; Zhang, S. *J. Phys. Chem. B* **2013**, *117*, 9042–9049.
- (38) Zhao, Y.; Liu, X.; Wang, J.; Zhang, S. *Carbohydr. Polym.* **2013**, *94*, 723–730.
- (39) Gross, A. S.; Bell, A. T.; Chu, J.-W. *J. Phys. Chem. B* **2011**, *115*, 13433–13440.
- (40) Gross, A. S.; Bell, A. T.; Chu, J.-W. *Phys. Chem. Chem. Phys.* **2012**, *14*, 8425–8430.
- (41) Caleman, C.; Maaren, P. J. V.; Hong, M.; Hub, J. S.; Costa, L. T.; van der Spoel, D. *J. Chem. Theory Comput.* **2012**, *8*, 61–74.
- (42) Berens, P. H.; Mackay, D. H. J.; White, G. M.; Wilson, K. R. *J. Chem. Phys.* **1983**, *79*, 2375–2389.
- (43) Lin, S. T.; Blanco, M.; Goddard, W. A., III *J. Chem. Phys.* **2003**, *119*, 11792.
- (44) Pascal, T. A.; Lin, S. T.; Goddard, W. A., III *Phys. Chem. Chem. Phys.* **2011**, *13*, 169–181.
- (45) Waheed, Q.; Edholm, O. *J. Chem. Theory Comput.* **2011**, *7*, 2903–2909.
- (46) Wohlert, J. *J. Phys. Chem. B* **2014**, *118*, 5365–5373.
- (47) Lopes, J. N. C.; Padua, A. a. H.; Shimizu, K. *J. Phys. Chem. B* **2008**, *112*, 5039–5046.
- (48) Vanommenslaeghe, K.; Hatcher, E.; Acharya, C.; Kundu, S.; Zhong, S.; Shim, J.; Darian, E.; Lopes, P.; Vorobyov, I.; Mackerell, A. D., Jr. *J. Comput. Chem.* **2010**, *31*, 671–690.
- (49) Wang, J.; Wolf, R. M.; Caldwell, J. W.; Kollman, P. A.; Case, D. A. *J. Comput. Chem.* **2004**, *25*, 1157–1174.
- (50) Fox, T.; Kollman, P. A. *J. Phys. Chem. B* **1998**, *102*, 8070–8079.
- (51) Hess, B.; Kutzner, C.; van der Spoel, D.; Lindahl, E. *J. Chem. Theory Comput.* **2008**, *4*, 435–447.
- (52) Brooks, B. R.; Brooks, C. L., III; Mackerell, A. D., Jr.; Nilsson, L.; Petrella, R. J.; Roux, B.; Won, Y.; Archontis, G.; Bartels, C.; Boresch, S.; Caisch, A.; Caves, L.; Cui, Q.; Dinner, A. R.; Feig, M.; Fischer, S.; Gao, J.; Hodoscek, M.; Im, W.; Kuczera, K.; Lazaridis, T.; Ma, J.; Ovchinnikov, V.; Paci, E.; Pastor, R. W.; Post, C. B.; Pu, J. Z.; Schaefer, M.; Tidor, B.; Venable, R. M.; Woodcock, H. L.; Wu, X.; Yang, W.; York, D. M.; Karplus, M. *J. Comput. Chem.* **2009**, *30*, 1545–1614.
- (53) Darden, T.; York, D.; Pedersen, L. *J. Chem. Phys.* **1993**, *98*, 10089–10092.
- (54) Essmann, U.; Perera, L.; Berkowitz, M. L.; Darden, T.; Lee, H.; Pedersen, L. G. *J. Chem. Phys.* **1995**, *103*, 8577–8592.
- (55) Stillinger, F. H.; Rahman, A. *J. J. Chem. Phys.* **1974**, *60*, 1545–1557.
- (56) Nosé, S.; Klein, M. L. *J. Chem. Phys.* **1983**, *78*, 6928–6939.
- (57) Hoover, W. G. *Phys. Rev. A* **1985**, *31*, 1695–1697.
- (58) Parrinello, M.; Rahman, A. *J. Appl. Phys.* **1981**, *52*, 7182–7190.
- (59) Nosé, S. *Mol. Phys.* **1984**, *52*, 255–268.
- (60) Hess, B. *J. Chem. Theory Comput.* **2008**, *4*, 116–122.
- (61) van Gunsteren, W. F.; Berendsen, H. J. C. *Mol. Phys.* **1977**, *34*, 1311–1327.
- (62) Beutler, T. C.; Mark, A. E.; van Schaik, R. C.; Greber, P. R.; van Gunsteren, W. F. *Chem. Phys. Lett.* **1994**, *222*, 529–539.
- (63) Bennet, C. H. *J. Comput. Phys.* **1976**, *22*, 245–268.
- (64) Sugita, Y.; Okamoto, Y. *Chem. Phys. Lett.* **1999**, *314*, 141–151.
- (65) Holbrey, J. D.; Reichert, W. M.; Nieuwenhuyzen, M.; Johnson, S.; Seddon, K. R.; Rogers, R. D. *Chem. Commun.* **2003**, *2003*, 1636.
- (66) Saha, S.; Hayashi, S.; Kobayashi, A.; Hamaguchi, H. *Chem. Lett.* **2003**, *32*, 740–741.
- (67) Fredlake, C. P.; Crosthwaite, J. M.; Hert, D. G.; Aki, S. N. V. K.; Brennecke, J. F. *J. Chem. Eng. Data* **2004**, *49*, 954–964.
- (68) Yamamuro, O.; Minamimoto, Y.; Inamura, Y.; Hayashi, S.; Hamaguchi, H. *Chem. Phys. Lett.* **2006**, *423*, 371–375.
- (69) Zhang, M.; Kamavaram, V.; Reddy, R. G. *J. Phase Equilib. Diffusion* **2005**, *26*, 124–130.
- (70) Wang, J.; Chakraborty, B.; Eapen, J. *Phys. Chem. Chem. Phys.* **2014**, *16*, 3062–3069.
- (71) Kick, M.; Keil, P.; König, A. *Fluid Phase Equilib.* **2013**, *338*, 172–178.
- (72) Nishikawa, K.; Wang, S.; Katayanagi, H.; Hayashi, S.; Hamaguchi, H.; Koga, Y.; Tozaki, K. *J. Phys. Chem. B* **2011**, *111*, 4894–4900.
- (73) Verevkin, S. P.; Zaitsau, D. H.; Emelyanenko, V. N.; Ralys, R. V.; Yermalayeu, A. V. *Thermochim. Acta* **2013**, *562*, 84–95.
- (74) Hess, B. *J. Chem. Phys.* **2002**, *116*, 209–217.
- (75) Fendt, S.; Padmanabhan, S.; Blanche, H. W.; Prausnitz, J. M. *J. Chem. Eng. Data* **2011**, *56*, 31–34.
- (76) Hu, Z.; Margulis, C. *J. Acc. Chem. Res.* **2007**, *40*, 1097–1105.
- (77) Tokuda, H.; Hayamizu, K.; Ishii, K.; Susan, M. A. B. H.; Watanabe, M. *J. Phys. Chem. B* **2004**, *108*, 16593–16600.
- (78) Tsuzuki, S.; Shinoda, W.; Saito, H.; Mikami, M.; Tokuda, H.; Watanabe, M. *J. Phys. Chem. B* **2009**, *113*, 10641–10649.
- (79) Kowsari, M. H.; Alavi, S.; Ashrafizaadeh, M.; Najafi, B. *J. Chem. Phys.* **2008**, *129*, 224508.
- (80) Urahata, S. M.; Ribeiro, M. C. C. *J. Chem. Phys.* **2005**, *122*, 024511.
- (81) Urahata, S. M.; Ribeiro, M. C. C. *J. Chem. Phys.* **2006**, *124*, 074513.
- (82) Yeh, I.; Hummer, G. *J. Phys. Chem. B* **2004**, *108*, 15873–15879.
- (83) Martinelli, A.; Maréchal, M.; Östlund, Å.; Cambedouzou, J. *Phys. Chem. Chem. Phys.* **2013**, *15*, 5510–5517.
- (84) Schröder, C.; Haberler, M.; Steinhauser, O. *J. Chem. Phys.* **2008**, *128*, 134501.
- (85) Zech, O.; Stoppa, A.; Buchner, R.; Kunz, W. *J. Chem. Eng. Data* **2010**, *55*, 1774–1778.
- (86) Vila, J.; Fernandez-Castro, B.; Rilo, E.; Carrete, J.; Dominguez-Perez, M.; Rodriguez, J. R.; Garcia, M.; Varela, L. M.; Cabeza, O. *Fluid Phase Equilib.* **2012**, *320*, 1–10.
- (87) Calvar, N.; González, B.; Domnguez, a.; Tojo, J. *J. Solution Chem.* **2006**, *35*, 1217–1225.
- (88) Calvar, N.; González, B. n.; Gómez, E.; Domnguez, A. *J. Chem. Eng. Data* **2006**, *51*, 2178–2181.
- (89) Jahangiri, S.; Taghikhani, M.; Behnejad, H.; Ahmadi, S. *Mol. Phys.* **2008**, *106*, 1015–1023.
- (90) Méndez-Morales, T.; Carrete, J.; Cabeza, O.; Gallego, L. J.; Varela, L. M. *J. Phys. Chem. B* **2011**, *115*, 11170–11182.
- (91) Lynden-Bell, R. M.; Atamas, N. A.; Vasilyuk, A.; Hanke, C. G. *Mol. Phys.* **2002**, *100*, 3225–3229.
- (92) Renon, H.; Prausnitz, J. M. *AIChE J.* **1968**, *14*, 135–144.
- (93) Verevkin, S. P.; Vasiltsova, T. V.; Bich, E.; Heintz, A. *Fluid Phase Equilib.* **2004**, *218*, 165–175.

- (94) Verevkin, S. P.; Safarov, J.; Bich, E.; Hassel, E.; Heintz, A. *Fluid Phase Equilib.* **2005**, *236*, 222–228.
- (95) Lazaridis, T.; Paulaitis, M. E. *AIChE J.* **1993**, *39*, 1051–1060.
- (96) Slusher, J. T. *Fluid Phase Equilib.* **1998**, *153*, 45–61.
- (97) Kobrak, M. N. *J. Phys. Chem. B* **2007**, *111*, 4755–4762.
- (98) Kobrak, M. N.; Li, H. *Phys. Chem. Chem. Phys.* **2010**, *12*, 1922–1932.
- (99) Tachida, H.; Taguchi, R.; Sato, Y.; Smith, R. L., Jr. *J. Chem. Eng. Data* **2011**, *56*, 923–928.
- (100) Zhang, S.; Sun, N.; He, X.; Lu, X.; Zhang, X. *J. Phys. Chem. Ref. Data* **2006**, *35*, 1475–1517.
- (101) Lopes, P. E. M.; Roux, B.; MacKerell, A. D., Jr. *Theor. Chem. Acc.* **2009**, *124*, 11–28.